Journal of Sound and Vibration 326 (2009) 438–455

Contents lists available at ScienceDirect

Journal of Sound and Vibration

journal homepage: www.elsevier.com/locate/jsvi

Active vibration control of a flexible beam using a non-collocated acceleration sensor and piezoelectric patch actuator

Zhi-cheng Qiu [a,*], Jian-da Han [b], Xian-min Zhang [a], Yue-chao Wang [b], Zhen-wei Wu [b]

[a] School of Mechanical and Automotive Engineering, South China University of Technology, Guangzhou 510641, PR China
[b] State Key Laboratory of Robotics, Shenyang Institute of Automation, Chinese Academy of Sciences, Shenyang 110016, PR China

ARTICLE INFO

Article history:
Received 21 November 2008
Received in revised form
28 March 2009
Accepted 30 May 2009
Handling Editor: J. Lam
Available online 24 June 2009

ABSTRACT

In this paper, the design of an acceleration sensor based active vibration control for a cantilever beam with bonded piezoelectric patches is studied. The problem of phase hysteresis and time delay caused by the non-collocated sensor/actuator pairs is considered. The system's dynamic model considering the non-collocated placement of the acceleration sensor and the piezoelectric patch actuator is derived. The phenomenon of phase hysteresis and time delay degrades the performance of the control system, or even induces instability. To solve the problem, an acceleration sensor based proportional feedback control algorithm and a sliding mode variable structure control algorithm with phase shifting technology are proposed, for suppressing the first two bending modes vibration of the beam. The stability of the proposed controllers was theoretically analyzed. The modal frequencies, phase hysteresis loops and phase lag values due to non-collocated placement of the acceleration sensor and the piezoelectric patch actuator are experimentally obtained, and the phase lag is compensated by using the phase shifting technology. Experiments are conducted to compare the above two active vibration control algorithms. Experimental results demonstrate that the presented acceleration sensor based control methods are effective.

1. Introduction

Lighter structures are increasingly needed for aerospace applications. Light structures are generally less rigid, so they are more susceptible to excessive vibration problems [1]. For example, the appendages of the large flexible space structures (LFSS) and space robotic systems usually have very low damping ratios and stiffness, so unwanted vibrations of the systems will be caused by external disturbances [2]. In order to meet the need for accurately pointing antenna and high end-position accuracy of the robotic arms, the issue on active vibration control for this kind of systems is more important than ever [3]. The challenging problem of active vibration control for such flexible beam systems must be solved.

During the past few decades, there has been considerable interest in the area of the active control of structural vibrations by using piezoelectric materials as sensors and actuators. The advantage of applying smart materials to control vibrations of an adaptive flexible structure is that the controller can adapt to system changes. The previous research works include dynamics modeling and control [4–28]. These methods are involved in the application of smart materials that utilize distributed piezoelectric actuators and sensors to suppress unwanted vibration in flexible structures. To design piezoelectric smart structures for active vibration control, both structural dynamics and control theory must be considered.

* Corresponding author. Tel.: +86 20 8711 4635; +86 20 8711 3431.
E-mail addresses: zhchqiu@scut.edu.cn, zhchqiu@126.com (Z.-c. Qiu).

0022-460X/$ - see front matter © 2009 Elsevier Ltd. All rights reserved.
doi:10.1016/j.jsv.2009.05.034

Bailey and Hubbard [4] proposed constant gain and constant amplitude control algorithms to perform vibration control of a piezoelectric cantilever beam. Fuller et al. [5] developed a dynamics model for piezoelectric flexible beam and plate structures. To actively control piezoelectric smart structures, Gardonio and Elliott [6] presented a theoretical analysis of the flexural response of a beam with a control system which implements direct velocity feedback (DVFB), using a collocated velocity sensor and force actuator or a practical closely located velocity sensor and piezoelectric patch sensor. Dong et al. [7] employed a linear-quadratic Gaussian (LQG) algorithm and Kalman filter identification technique. Xu and Koko [8] proposed the design of a LQG control based on finite element analysis (FEA). Goh and Caughey [9] proposed the use of positive position feedback (PPF) control scheme based on the modal displacement signal. The PPF controller is very effective in suppressing the specific vibration mode thus maximizing the damping in the targeted mode without destabilizing other modes [10]. Fanson et al. [10] performed experiments on a beam with piezoelectric materials using PPF strategy. However, when the frequencies used in the PPF controller are different from those of the structure, the performance of the PPF control is adversely affected. Baz and Poh [11] presented a modified independent modal space control (MIMSC) method. By using this method, one piezoelectric actuator can control several modes at the same time.

To cope with the existing model uncertainty, adaptive output feedback control [12], H_∞ control [13], nonlinear adaptive control methods [14] and hierarchical fuzzy methodology [15] were proposed. The controller designed is robust to a certain level of unmodeled dynamics or parameter uncertainty. The robustness achieved by even an H_∞ controller is dependent on the bound on uncertainty used in the design. To minimize the residual vibration, several control algorithms are presented. Qiu et al. [16] proposed the combining of PPF and PD control algorithm. Singh and Singhose [17] proposed the input shaping techniques. Shan et al. [18] presented a development of robust component synthesis vibration suppression method for control of flexible structures. Unlike the traditional input shaping method, a numerical optimization is used. For active control of rotating flexible manipulator, Cannon and Schmitz [19] used linear system control approaches utilizing end-point measurement to control a single-link flexible robot. Sun et al. [20] proposed a hybrid control algorithm to control the rotation of a flexible beam while suppressing the beam's vibration. The control law combines an enhanced PD feedback with a nonlinear differentiator to derive a high-quality velocity signal to control the gross motion of the beam, and a vibration control by PZT actuators bonded on the surface of the beam. Experimental and numerical results validate these theoretical analyses and control methods.

However, the aim of vibration control for distributed parameter system is to design the control methods based only on a limited number of modes that use much small numbers of actuators/sensors to control a large dimensional system. When the excitation of the residual modes by the actuators is the result of the active control system, this is known as control spillover [21]. Control spillover may occur if high frequency dynamics is ignored by modal truncation, and the spillover will cause instability in the closed-loop system [22]. Furthermore, these models always have parametric uncertainties, and these flexible structures are always disturbed by external disturbances. Therefore, a control system for vibration suppression in flexible structures should be robust to parametric uncertainties in both dynamics and external disturbances, and spillover phenomenon must be considered simultaneously [23]. Because of its simplicity and robustness to parametric uncertainties and external disturbances, variable structure control (VSC) is particularly attractive for nonlinear control problems [24,25]. Choi et al. [26] formulated a new discrete-time sliding mode controller and conducted experimental researches to alleviate chattering in vibration control of smart structures and also to achieve robustness to the system uncertainties.

The conventional sliding mode control systems are always limited to be used only for the systems with full-state feedback. In practice, full measurement of the state vector is not feasible and impractical. The technique is based on the sliding mode control algorithm designed by using direct output feedback [23,27]. The control law developed in this way is based on output feedback, so it does not require an estimator and is easy to implement [28,29]. Cao and Xu [30] applied a learning variable structure controller to suppress the vibration of a flexible one-link manipulator. Hu [31] investigated a hybrid control scheme for vibration reduction of flexible spacecraft during rotational maneuvers by using variable structure output feedback control for attitude control and smart materials for active vibration suppression.

To measure and control vibrations, an accelerometer is often used as sensor in flexible structures. Acceleration is often easier to measure than displacement or velocity. Kotnic and Yurkovich et al. [32] used acceleration feedback for the endpoint position control of a flexible robot arm. Gatti et al. [33] conducted active damping of a beam using physically collocated accelerometer and piezoelectric patch actuator. Preumont [28] addressed the case in which the output of the system is the acceleration and the control input is a force, by using collocated actuator and sensor pairs. He presented a compensator involving a second-order filter which also enjoys guaranteed stability and exhibits a larger roll-off at high frequency. He then considered the case of a single degree of freedom oscillator and extended the results to SISO systems with many modes and to MIMO systems. Han et al. [34] and Xu et al. [35] have conducted experiments on acceleration sensor based robust control for robots to improve the control accuracy of the trajectory tracking. Dumetz et al. [36] applied motor-position-based PD combined with positive acceleration feedback algorithm to control the axis of an industrial robot. The controller is robust with respect to the high frequency disturbances due to measurement noise or higher order vibration modes.

When an accelerometer is fixed at the tip of a beam, the outputs are the acceleration at the tip of the beam and the strain at the vicinity of the clamped side. Therefore, the system has non-minimum-phase zeros due to the non-collocated pair of sensor and actuator, and it poses challenging problem for controller design [37]. Chatterjee [38] presented a theoretical basis of vibration control strategy based on the time-delayed acceleration feedback control of linear and

nonlinear vibrations of mechanical oscillators. Qiu [39,40] presented a kind of acceleration sensor based combining nonlinear control algorithm to suppress the vibration of piezoelectric smart structure. Since the system has a non-collocated sensor/actuator pair, it is a non-minimum phase system. This will cause a phase hysteresis and time delay, which can not only degrade the performance of the control systems, but also induce instability in the closed-loop systems, due to unsynchronized control forces effect [41]. Thus, phase tuning technology must be applied to ensure the stability of the closed-loop control system. Whichever controller is used, the key problem is how to maintain the stability, robustness and performance of the closed-loop system. Tan et al. [42] explained explicitly the potential of acceleration measurements to achieve more precise motion control. By adopting adequate digital filtering techniques, the noise-related problems can be reduced to a level where the signal may be made available for direct analysis by the controller.

In practice, physical systems are inherently nonlinear [24]. Thus, all control systems are nonlinear to a certain extent. Because of the dead zone nonlinear characteristic of the system, the lower amplitude modal vibration near the equilibrium point is hard to be suppressed. Also, it is a challenge to design a non-collocated accelerometer based feedback controller because of the non-minimum phase characteristic and the very noisy signal of the measuring accelerometer. The phenomenon of control spillover will be caused due to noises and phase errors. Especially, it is difficult to design and implement a VSC controller by using acceleration signal for active control of flexible structures.

The aim of this paper is to suppress the vibrations of a flexible beam by using a non-collocated acceleration sensor and discrete PZT patch sensor/actuator, and the above-mentioned problems are considered for controller design. A second-order low-pass filter is introduced in the controller to eliminate high frequency noises and the problem of control spillover. Phase shifting technology is used to compensate for the phase lag due to the non-collocated placement of sensor/actuator pair. A combined controller is proposed to suppress both the larger and the lower amplitude vibrations quickly.

The contributions of this paper are as follows: (a) In order to suppress the first two bending modes' vibration of the beam, non-collocated acceleration based proportional feedback control and sliding mode variable structure control algorithms are proposed. By using phase shifting technology, the hysteresis and time delay are compensated for the first two bending modes. The problems of control "spillover" and high frequency noises are eliminated by introducing a second low-pass filter. And the combination algorithm of both the methods is proposed to suppress both the larger and the lower amplitude vibrations quickly. In this case, the selected control gain of the acceleration proportional control is not so larger, and then the stability and control spillover of the closed-loop system will not be affected due to much higher control gain. However, for suppressing the lower amplitude vibration, the combined method can supply much larger control effect compared to that of the proportional control. Therefore, the combined method can not only keep the proportional gain not so high for the larger amplitude vibration, but also keep at a certain control effect for the lower amplitude vibration. Thus, it can suppress the lower amplitude residual vibration quickly. Therefore, the combined method can overcome the problems of the system, such as dead zone nonlinearity. (b) Considering the phase lag and its compensation by phase shifting technology, the stability of the proposed acceleration proportional feedback control and the VSC control and the combined method are analyzed and proven by using the Hurwitz criterion and Lyapunov stability theory, respectively, and both the control schemes are guaranteed to be stable for the closed-loop control system. (c) Experiments are conducted to compare the results of the different control methods. Experimental results demonstrate the satisfactory closed-loop performance of the acceleration sensor based control method, and their stability and effectiveness are experimentally verified. Significantly, both the larger and the lower amplitude vibrations near the equilibrium point are suppressed by the presented control methods quickly.

The organization of this article is as follows. In Section 2, the governing equation of motion for acceleration sensor based piezoelectric flexible beam is derived. In Section 3, an acceleration proportional feedback control algorithm and a sliding mode variable structure control algorithm with phase shifting technology are presented to suppress the first two bending modes' vibration of the beam, and then their stabilities are analyzed. In Section 4, an experimental apparatus of piezoelectric smart cantilever beam for active vibration control is designed and built up. The modal frequencies and phase lag parameters with respect to the non-collocated beam system are experimentally identified by excitation analysis. Experimental identifications are conducted by using impulse excitation for the first bending mode and by persistent excitation for the second bending mode. The experimental research is carried out to suppress vibration by the above two control algorithms. Finally, the conclusions are presented in Section 5.

2. The system's model and modal analyses

2.1. Mathematical model

In this section, a mathematical model is derived for flexible beam structure equipped with an acceleration sensor and PZT actuator. The schematic diagram of the piezoelectric adaptive flexible uniform slender beam is shown in Fig. 1. Here, an accelerometer and one PZT patch are used as sensors, and four other PZT patches bonded perfectly and symmetrically on the top and the bottom surfaces of the host beam structure are in parallel and used as a one-channel actuator. The surface mounted PZT sensor/actuator patches are close to the clamped side of the beam. The accelerometer is mounted at the tip of the beam, adding the concentrated mass (payload) at the tip end of the beam. Pure bending moment is created from the PZT actuator due to perfect bond of PZT patches pair close to the clamped side of the beam in the spanwise direction [43].

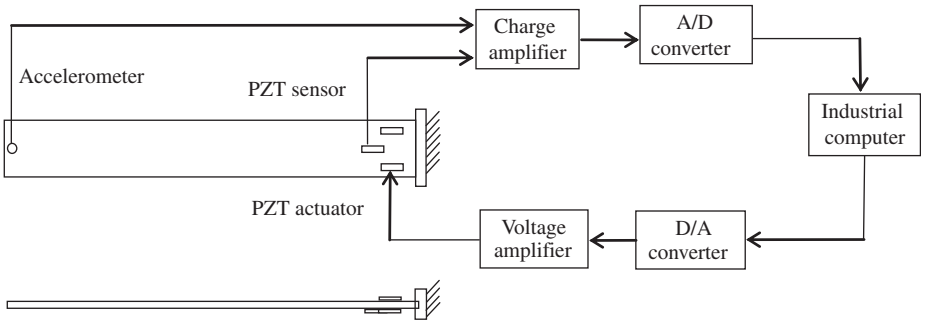

Fig. 1. Schematic diagram of the experimental setup.

For active vibration control, the modified independent modal space control method is adopted, that is to say, one PZT actuator can control several vibration modes simultaneously. In this paper, the bonded PZT actuator is used to control the first two bending modes of the beam.

By using the assumed modes method, the flexural deflection describing the motion of cantilever beam with tip mass system can be expressed as

$$w(x,t)=\sum_{i=1}^{n\to\infty}\Phi_i(x)q_i(t),\quad i=1,2,\ldots,n, \tag{1}$$

where $w(x,t)$ is the transverse displacement; q_i and Φ_i are the generalized coordinate and modal function of the ith mode, respectively; and n is the modal number; and $0\le x\le L$, L is the length of the uniform beam.

The mode shape function of the clamped beam with tip concentrated mass is expressed as [44]

$$\Phi_i(x)=C_i\left\{\cosh\left(\frac{\beta_i}{L}x\right)-\cos\left(\frac{\beta_i}{L}x\right)-\frac{\cosh(\beta_i)+\cos(\beta_i)}{\sinh(\beta_i)+\sin(\beta_i)}\times\left[\sinh\left(\frac{\beta_i}{L}x\right)-\sin\left(\frac{\beta_i}{L}x\right)\right]\right\}, \tag{2}$$

where C_i is a constant and β_i is the minimum positive solution of the following equation:

$$1+\cosh(\beta_i)\cos(\beta_i)+\frac{m_t\beta_i}{\rho_bA_bL}[\sinh(\beta_i)\cos(\beta_i)-\cosh(\beta_i)\sin(\beta_i)]=0, \tag{3}$$

where ρ_b and A_b are the mass density and the cross-sectional area of the beam, respectively; ρ_bA_b is the mass per unit length; and m_t denotes the mass of the tip mass.

According to Ref. [5], the equation of motion of the piezoelectric cantilever beam becomes

$$\frac{\partial^2}{\partial x^2}\left[E_bI_b\frac{\partial^2w(x,t)}{\partial x^2}\right]+\rho_bA_b\ddot{w}(x,t)=E_bI_bK^f\varepsilon_{pe}[\delta'(x-x_2)-\delta'(x-x_1)], \tag{4}$$

where E_b is Young's modulus of the beam; I_b is the cross-sectional moment of inertia about the neural axis of the beam, $I_b=b_bh_b^3/12$, where b_b is the width and h_b is the height (thickness) of the beam, respectively; $\delta'(\cdot)$ represents the derivative of the Dirac delta function with respect to its argument; x_1 and x_2 are the coordinates of the piezoelectric patch actuator's both sides in the X-direction; $\varepsilon_{\rm pe}$ is the resultant strain in the X-direction when the voltage V_a is applied in the Z-direction, and $\varepsilon_{\rm pe}=(d_{31}/h_a)V_a$; where d_{31} and h_a denote the piezoelectric strain constant and the thickness of the PZT actuator, respectively; and K^f is the material-geometric constant, and it is described as [5]

$$K^f=\frac{3E_{\rm pe}[(h_b+h_a)^2-h_b^2]}{2\{E_{\rm pe}[(h_b+h_a)^3-h_b^3]+E_bh_b^3\}}, \tag{5}$$

where $E_{\rm pe}$ is Young's modulus of the PZT actuator.

For the smart beam, the total charge of the piezoelectric sensor is

$$q(t)=-e_{31}b_sr\int_0^{L_s}\frac{\partial^2w(x,t)}{\partial x^2}\,{\rm d}x, \tag{6}$$

where e_{31} denotes the piezoelectric stress constant of the piezoelectric sensor; b_s is the width of the piezoelectric sensor patch; r denotes the distance between the middle plane of the sensor patch and that of the host beam structure; and L_s is the total length of the piezoelectric patch sensor.

The measured acceleration signal by the fixed accelerometer is

$$y_a = \ddot{w}(l,t) = \sum_{i=1}^{n\to\infty} \Phi_i(l)\ddot{q}_i(t), \tag{7}$$

where l is the distance between the fixed point of the accelerometer and the clamped end.

The state-space representation of the piezoelectric control system can be expressed as

$$\frac{\mathrm{d}\mathbf{z}}{\mathrm{d}t} = \mathbf{A}_p\mathbf{z} + \mathbf{B}_p u, \tag{8}$$

$$y_p = \mathbf{C}_p\mathbf{z}, \tag{9}$$

$$y_a = \mathbf{C}_a\frac{\mathrm{d}\mathbf{z}}{\mathrm{d}t}, \tag{10}$$

where $\mathbf{z} = [q_1 \cdots q_n \ \dot{q}_1 \cdots \dot{q}_n]^{\mathrm{T}}$ is the state vector; $\mathbf{A}_p$ is the state matrix; $\mathbf{B}_p$ is the input matrix; $\mathbf{C}_p$ is the output matrix about PZT patch sensor; $\mathbf{C}_a$ is the output matrix about acceleration sensor; u is the control input voltage; y_p is the measured output of the PZT patch sensor; and y_a is the measured output of the acceleration sensor. They are written as follows:

$$\mathbf{A}_p = \begin{bmatrix} \mathbf{0} & \boldsymbol{I} \\ -\boldsymbol{\Omega}^2 & -2\boldsymbol{\zeta}\boldsymbol{\Omega} \end{bmatrix}, \quad \mathbf{A}_p \in \Re^{2n\times 2n},$$

where $\boldsymbol{\Omega} = \mathrm{diag}(\omega_i)$, $\boldsymbol{\zeta} = \mathrm{diag}(\xi_i)$, where ω_i and ξ_i are the natural modal frequency and damping ratio of the ith mode, respectively;

$$\mathbf{B}_p = \mathbf{M}_b^{-1}[0\cdots 0 \ P_1\cdots P_i\cdots P_n]^{\mathrm{T}}, \quad \mathbf{B}_p \in \Re^{2n\times 1}; \quad \mathbf{C}_p = [S_1\cdots S_i\cdots S_n \ 0\cdots 0], \quad \mathbf{C}_p \in \Re^{1\times 2n},$$
$$\mathbf{C}_a = [0\cdots 0, \ \Phi_1(l)\cdots\Phi_n(l)], \quad \mathbf{C}_a \in \Re^{1\times 2n};$$

where $P_j = -c[\Phi_j'(x_2) - \Phi_j'(x_1)]$ is the parameter for the jth mode of the piezoelectric actuator pairs and the parameter c is expressed as [5]

$$c = \frac{3d_{31}E_bI_bE_{\mathrm{pe}}[(h_b+h_{\mathrm{pe}})^2 - h_b^2]}{2h_{\mathrm{pe}}\{E_{\mathrm{pe}}[(h_b+h_{\mathrm{pe}})^3 - h_b^3] + E_bh_b^3\}},$$

where d_{31} is the piezoelectric strain constant; $S_i = -K_s[\Phi_i'(x_2) - \Phi_i'(x_1)]$ is the element for the ith mode of the piezoelectric sensor; $K_s = -e_{31}b_sr$ is the sensing factor; and N_s and N_a are the number of the piezoelectric sensors and actuators, respectively. The ith row and the jth column element of the mass matrix $\mathbf{M}_b$ for the beam is expressed as $\mathbf{M}_{bij} = \rho_bA_b\int_0^L \Phi_i(x)\Phi_j(x)\,\mathrm{d}x$.

2.2. Modal shapes and finite element analysis

The beam is made of fiberglass colophony. The geometrical size of the beam is: length $L = 0.62$ m, width $b = 0.16$ m, and thickness $h_b = 1.78$ mm. Young's modulus, Poisson's ratio and mass density are $E_b = 34.64$ Gpa, $\nu_b = 0.33$ and $\rho_b = 1865\,\mathrm{kg/m^3}$, respectively.

In order to measure the tip acceleration, an accelerometer is used. The acceleration sensor is fixed at the concrete point close to the tip side of the beam by a bolt. The distance between the clamped side and its central point is $l = 0.60$ m. The mass of the accelerometer is 50 g.

The piezoelectric patches are bonded to the top and bottom surfaces and close to the clamped end of the host beam structure using strong epoxy adhesive material. The PZT patches are 50 mm × 15 mm × 1 mm in size. The parameters of the PZT patches are as follows: Young's elastic modulus $E_{\mathrm{pe}} = 6.3\times10^{10}\,\mathrm{N/m^2}$, Poisson's ratio $\nu_{\mathrm{pe}} = 0.30$, and density $\rho_{\mathrm{pe}} = 7650\,\mathrm{kg/m^3}$; the piezoelectric strain constant $d_{31} = d_{32} = -166\times10^{-12}$, $d_{36} = 0$ m/V, respectively. The coordinates of the bonded PZT actuator patches in the x-direction are $x_1 = 0.02$ m and $x_2 = 0.07$ m, respectively. The coordinates of PZT sensor patch are $x_3 = 0.05$ m and $x_4 = 0.10$ m, respectively.

Theoretically, the flexible beam is an infinite-dimensional system. However, the number of excited modes is finite due to finite energy. Hence, only the first two bending modes are considered for controller design and stability analysis in Section 3. When an acceleration sensor is mounted at the tip of the beam as a concentrated mass, then the minimum positive solution of Eq. (3) can be obtained as $\beta_1 = 1.664$ and $\beta_2 = 4.320$, respectively. When the accelerometer is taken away, and the effects of the PZT patches are neglected, then it can be just regarded as a cantilever beam. The minimum positive solution β_i of Eq. (3) for the first two bending modes are $\beta_1 = 1.875$ and $\beta_2 = 4.694$, respectively.

The mode shapes for the above two cases are shown in Fig. 2. They are the calculated results of mode shapes with and without a concentrated mass at the tip of the beam, respectively. The results for the first case are the two bending mode shapes that are plotted by two dashed lines. The results for the second case are the two bending mode shapes plotted by two solid lines. From Fig. 2, it can be seen that the concentrated mass will affect the mode shapes to some degree.

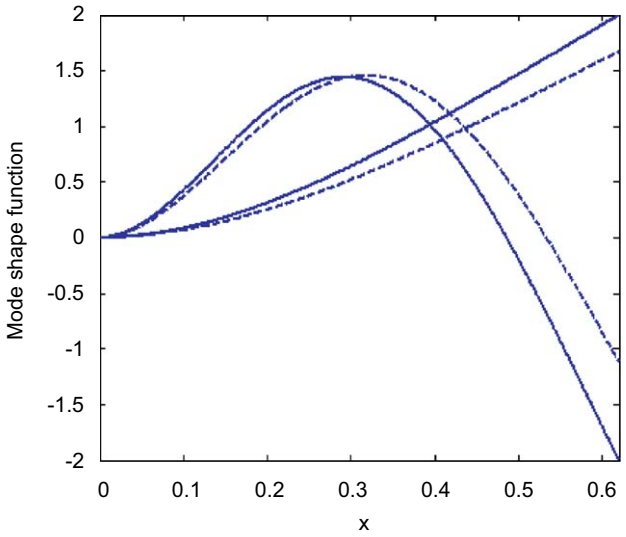

Fig. 2. Mode shapes of the beam with and without accelerometer.

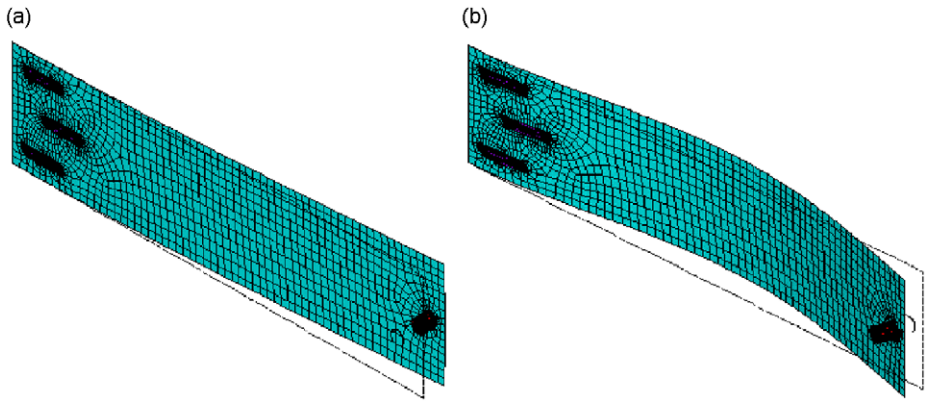

Fig. 3. Mode shapes of the piezoelectric beam structure with an acceleration sensor: (a) the first bending mode and (b) the second bending mode.

According to the derivative of Eq. (2), one can obtain the following relationship: $[\Phi_1'(x_2) - \Phi_1'(x_1)] = 0.655$ and $[\Phi_2'(x_2) - \Phi_2'(x_1)] = 3.313$. These results will be used in the stability analysis of acceleration feedback control in Section 3.1.

The natural frequency of the ith mode is

$$\omega_i = \sqrt{\frac{E_b I_b}{\rho_b A_b L^4}}(\beta_i)^2. \tag{11}$$

By using Eq. (11), the natural frequencies of the first two bending modes of the beam are $\omega_1 = 3.22$ Hz and $\omega_2 = 20.20$ Hz for the beam without a concentrated mass, respectively. And they are $\omega_1 = 2.54$ Hz and $\omega_2 = 17.11$ Hz for the beam with a concentrated mass, respectively.

Fig. 3 illustrates the first and the second bending mode shapes of the piezoelectric cantilever beam with an accelerometer by employing finite element analysis (FEA). Here, the accelerometer can be seen as centralized mass at the fixed point. The first and the second bending mode shapes are shown in Fig. 3(a) and (b); and their frequencies calculated by FEA are 2.55 and 17.74 Hz, respectively. Compared the calculated results by using Eq. (11) with those of FEA, it can be seen that they are approximately equal. The results of FEA are in good agreement with the calculated results. Thus, the bonded PZT patches do not significantly affect the dynamics of the beam. So the added stiffness and mass effects of the PZT patches can be neglected in the modal analysis.

3. Control algorithms design and stability analysis

3.1. Acceleration sensor based proportional feedback control

The control law developed in this paper is based on the signal measured by an acceleration sensor. As shown in Fig. 1, the system outputs are the acceleration at the tip of the beam and the strain at the vicinity of the clamped side measured by the accelerometer and the PZT patch sensor, respectively. When the accelerometer is used as a sensor, the system has non-minimum phase zeros due to the non-collocated pair of the sensor and the actuator. The non-minimum phase zeros do not affect the magnitude significantly. However, they do have substantial influence on the phase [37]. The phase lag and time delay will degrade the performance of the control system and will induce instability. Therefore, it poses challenging problems for controller design due to the non-collocated pair of the acceleration sensor and the PZT actuator. In this paper, a phase shifting method is used to compensate for the phase lag and time delay of the acceleration feedback control. In addition, because the acceleration sensor measured signal comprises a large amount of noises, a low-pass filter is used to filter out the high frequency noise of the sensor signal. Also, the problem of control "spillover" can be significantly reduced by introducing the second low-pass filter in the closed-loop system.

The proportional feedback control based on acceleration signal is

$$u = -K_a y_a(t-\Delta t)\frac{a}{s+a}\frac{b}{s+b} = -K_a \ddot{w}(l,t-\Delta t)\frac{a}{s+a}\frac{b}{s+b} = -K_a \sum_{i=1}^{n} \Phi_i(l)\ddot{q}_i(t-\Delta t)\frac{a}{s+a}\frac{b}{s+b}, \tag{12}$$

where s is Laplace operator; a and b are the corner frequencies of a first-order low-pass filter; Δt is the phase tuning time; and $K_a > 0$ is the proportional gain of the acceleration feedback control law.

Here, Δt is obtained by an experimental identification method. By introducing the phase tuning time Δt, a time delay effect is incorporated in the controller design, and the phase lag for the first two bending modes due to the non-collocated sensor/actuator pair can be compensated for. Thus, the classical way of alleviating the effect of the flexible modes in non-collocated control is to supplement phase shifting compensator so that stability problem will not arise. Then, the stability of the control algorithm is analyzed for the first and the first two bending modes by using the acceleration output proportional feedback control law.

Let

$$\omega_f = \sqrt{ab}, \tag{13a}$$

$$\xi_f = \frac{a+b}{2\sqrt{ab}}, \tag{13b}$$

where ω_f and ξ_f are the corner frequency and the damping ratio of the second-order filter, respectively. In this way, a second-order low-pass filter can be represented by two one-order low-pass filters equivalently.

They meet the following relationship:

$$\frac{a}{s+a}\frac{b}{s+b} = \frac{ab}{s^2+(a+b)s+ab} = \frac{\omega_f^2}{s^2+2\xi_f\omega_f s+\omega_f^2}. \tag{14}$$

When the second-order filter is implemented in controller design, the considered natural frequency of the structure mode should be less than that of the filter, that is to say, $\omega_i < \omega_f$. In this paper, the first two bending modes are considered; so in our model, there is $\omega_2 < \omega_f$.

$$u = -K_a \sum_{i=1}^{n} \Phi_i(l)\ddot{q}_i(t-\Delta t)\frac{\omega_f^2}{s^2+2\xi_f\omega_f s+\omega_f^2}. \tag{15}$$

On the basis of the previous research work of Preumont [28], the stability of the proposed acceleration feedback control is analyzed. The stability analysis of the non-collocated acceleration output proportional feedback control includes two cases. First, we consider that only the first bending mode is excited; second, the first two bending modes are both excited simultaneously. From Eqs. (8) and (10), it can be obtained that the equation of motion for the first bending mode is as follows:

$$\ddot{q}_1 + 2\xi_1\omega_1\dot{q}_1 + \omega_1^2 q_1 = \frac{-c[\Phi_1'(x_2) - \Phi_1'(x_1)]}{\rho_b A_b \int_0^L \Phi_1(x)^2\,dx}u. \tag{16}$$

The presented control algorithm that is expressed as Eq. (15) can also be expressed by the time-domain form as

$$\ddot{a}_c + 2\xi_f\omega_f\dot{a}_c + \omega_f^2 a_c = \omega_f^2\Phi_1(l)\ddot{q}_1(t-\Delta t), \tag{17}$$

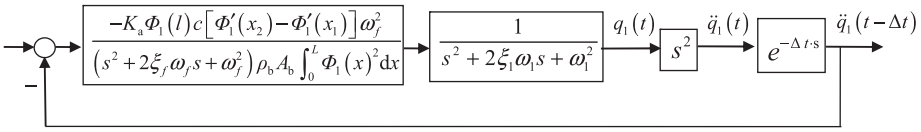

Fig. 4. Block diagram of the acceleration feedback control for the first bending mode.

$$u = -K_a a_c, \tag{18}$$

where a_c is the acceleration signal corrected by phase shifting and a second low-pass filter technology.

The block diagram of the phase shifting acceleration feedback control for the first bending mode is shown in Fig. 4. The closed-loop characteristic equation is

$$(s^2+2\xi_1\omega_1 s+\omega_1^2)(s^2+2\xi_f\omega_f s+\omega_f^2)\rho_b A_b\int_0^L\Phi_1(x)^2\,dx - K_a\Phi_1(l)c[\Phi_1'(x_2)-\Phi_1'(x_1)]\omega_f^2 e^{-\Delta t\cdot s}s^2 = 0, \tag{19}$$

where $\rho_b A_b\int_0^L\Phi_1(x)^2\,dx>0$; for the first bending mode, there are the following relationships: $\Phi_1(l)>0$, $c<0$, $[\Phi_1'(x_2)-\Phi_1'(x_1)]>0$. The generalized acceleration coordinate of the first bending mode can be expressed as $\ddot{q}_1 = A_1\sin(\omega_1 t+\varphi_1)$. When the phase shifting angle is equal to the phase reverse angle of "−180°", the gain is multiplied by "−1". And according to the experimental identification and compensation in Section 4.2, the phase shifting of the first bending mode is $\Delta t=-28.8$ ms and $\Delta\phi_1=-27.36°$. Therefore, phase shifting will not be multiplied by negative one for the first bending mode. Furthermore, there is $-\Phi_1(l)c[\Phi_1'(x_2)-\Phi_1'(x_1)]\omega_f^2 e^{-\Delta t\cdot s}>0$.

Let $\Psi = -\Phi_1(l)c[\Phi_1'(x_2)-\Phi_1'(x_1)]\omega_f^2 e^{-\Delta t\cdot s}/(\rho_b A_b\int_0^L\Phi_1(x)^2\,dx)$, and from the above analysis, there is $\Psi>0$. Then Eq. (19) yields

$$(s^2+2\xi_1\omega_1 s+\omega_1^2)(s^2+2\xi_f\omega_f s+\omega_f^2)+K_a\Psi s^2 = 0. \tag{20}$$

Using the Hurwitz criterion, one can check that the closed-loop system is always stable for $K_a>0$.

When the first two bending modes are considered simultaneously, the structure equation for the first bending mode is expressed by Eq. (16); and that of the second bending mode is

$$\ddot{q}_2+2\xi_2\omega_2\dot{q}_2+\omega_2^2 q_2 = \frac{-c[\Phi_2'(x_2)-\Phi_2'(x_1)]}{\rho_b A_b\int_0^L\Phi_2(x)^2\,dx}u, \tag{21}$$

$$\ddot{a}_c+2\xi_f\omega_f\dot{a}_c+\omega_f^2 a_c = \omega_f^2[\Phi_1(l)\ddot{q}_1(t-\Delta t)+\Phi_2(l)\ddot{q}_2(t-\Delta t)], \tag{22}$$

$$u = -K_a a_c. \tag{23}$$

According to Eq. (8), there are $B_{p1}=-c[\Phi_1'(x_2)-\Phi_1'(x_1)]/(\rho_b A_b\int_0^L\Phi_1(x)^2\,dx)$ and $B_{p2}=-c[\Phi_2'(x_2)-\Phi_2'(x_1)]/(\rho_b A_b\int_0^L\Phi_2(x)^2\,dx)$. Now, let us analyze the case for the second mode. For the second bending mode, there are the following relationships: $\rho_b A_b\int_0^L\Phi_2(x)^2\,dx>0$, $c<0$, $\Phi_2(l)<0$, $[\Phi_2'(x_2)-\Phi_2'(x_1)]>0$. The generalized acceleration coordinate of the second bending mode can be expressed as $\ddot{q}_2 = A_2\sin(\omega_2 t+\varphi_2)$. And according to the experimental identification and compensation in Section 4.2, the phase shifting of the first bending mode is $\Delta t=-28.8$ ms and $\Delta\phi_2=-170.2°$. Since the phase shifting angle is close to the phase reverse angle of "−180°", the gain is multiplied by "−1". Therefore, phase shifting is multiplied by negative one for the second bending mode. Furthermore, there is $-\Phi_2(l)c[\Phi_2'(x_2)-\Phi_2'(x_1)]\omega_f^2 e^{-\Delta t\cdot s}\times(-1)>0$.

The block diagram of the phase shifting acceleration feedback control for the first two bending modes is shown in Fig. 5. For acceleration based controller design, phase shifting technology is applied by using the parameters obtained from experimental identification. According to the improved individual modal space control and orthogonality for the first and the second modes, one can check that the closed-loop system is always stable for the first two bending modes when $K_a>0$.

In practice, piezoelectric accelerometers use charge amplifiers which behave as high-pass filters [28]. In this paper, the corner frequency of the charge amplifier's high-pass filter is set as 0.03 Hz, but the modal frequency of the first bending mode is $\omega_1=2.50$ Hz. Therefore, this does not significantly affect the characteristics because the corner frequency of the charge amplifier is well below the vibration modes of the structure. Because the experimental frequency of the second bending mode is $\omega_2=16.41$ Hz, it is reasonable to set the corner frequencies of the low-pass filters at 35 and 20 Hz for the experimental research. In addition, since there is a phase shift between the original and the filtered acceleration signals. The phase shift should be compensated for on the experimental research.

3.2. Acceleration signal based sliding mode control

Many of the sliding-mode control strategies require full-state feedback. But, all the states of the system are not always available for measurement. In practice, the output of the system is always a measurable quantity. Therefore, sensor output

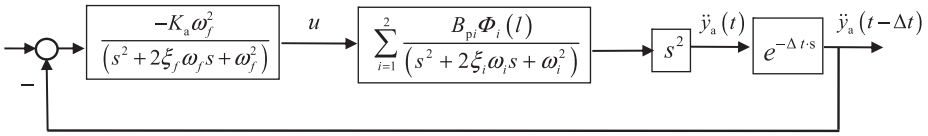

Fig. 5. Block diagram of the acceleration feedback control for the first two bending modes.

feedback based sliding mode control strategy is attractive and practical due to its easy implementation compared with full-state feedback based algorithms [23,27,29].

In Section 3.1, we show that the introducing phase shifting time Δt can compensate for the phase lag due to the non-collocated placement of the acceleration sensor for the first and the second bending modes. When sliding mode variable structure control methods are designed to suppress the vibration of the first two bending modes, the sliding variable of acceleration signal s_a is chosen as the integration of the measurements of the acceleration sensor,

$$s_a = c_1 \int_0^t y_a(t-\Delta t)\,\mathrm{d}t, \tag{24}$$

where c_1 is a constant, and its scope is 1–2, and $c_1 = 1$ in this paper; and Δt is the phase tuning time compensating for the phase lag time due to non-collocated placement of the acceleration sensor and the PZT actuator. It can be obtained from experimental identification of the parameters.

Remark. Generally, the sliding surface of the VSC is composed of both the signal and its derivative. However, the signal measured by acceleration sensor comprises a large amount of measured noises, and the derivative of such a signal will cause much larger amount of noises. The problems of instability and control spillover of the closed-loop system will be caused due to noises. Thus, we do not use the derivative of acceleration sensor measured signal for controller design. To select the sliding surface, the integration of acceleration signal is used for controller design.

The equivalent control u_{eq} is obtained from the condition $\dot{s}_a = 0$, that is

$$\dot{s}_a = c_1 y_a(t-\Delta t) = c_1 \mathbf{C}_a(\mathbf{A}_p \mathbf{z}(t-\Delta t) + \mathbf{B}_p u) = 0 \tag{25}$$

yields

$$u_{\mathrm{eq}} = -(\mathbf{C}_a\mathbf{B}_p)^{-1}\mathbf{C}_a\mathbf{A}_p\mathbf{z}(t-\Delta t). \tag{26}$$

To accommodate for "real-world" uncertainties, and parametric errors and disturbance effects, a variable structure control switch term is added to Eq. (26). Therefore, the total control is expressed as

$$u = u_{\mathrm{eq}} + u_{\mathrm{vss}}, \tag{27}$$

where the variable structure control law u_{vss} is written as

$$u_{\mathrm{vss}} = -Q\,\mathrm{sgn}(s_a) \tag{28}$$

and where Q is a positive constant; $\mathrm{sgn}(*)$ is sign function, and it is

$$\mathrm{sgn}(s_a) = \begin{cases} +1 & \text{if } s_a > 0, \\ 0 & \text{if } s_a = 0, \\ -1 & \text{if } s_a < 0. \end{cases} \tag{29}$$

In essence, to achieve perfect control performance, the system trajectories have to converge to s_a in finite time and stay on s_a afterwards. The reaching condition is expressed mathematically as [24,45]

$$\frac{1}{2}\frac{\mathrm{d}}{\mathrm{d}t}s_a^2 \le -\eta|s_a|, \tag{30}$$

where η is a strictly positive design parameter.

From Eq. (24), one can obtain

$$\begin{aligned} s_a\dot{s}_a &= s_a c_1 y_a(t-\Delta t) = s_a c_1 \mathbf{C}_a(\mathbf{A}_p\mathbf{z}(t-\Delta t) + \mathbf{B}_p u_{\mathrm{vss}}) \\ &= s_a c_1 \mathbf{C}_a(\mathbf{A}_p\mathbf{z}(t-\Delta t) - Q\mathbf{B}_p\,\mathrm{sgn}(s_a)) \le -\eta|s_a|. \end{aligned} \tag{31}$$

From Eq. (31), Q should be determined such that Eq. (30) is automatically satisfied. And from Eq. (31) one can obtain

$$Q \ge (c_1\mathbf{C}_a\mathbf{B}_p)^{-1}(\eta+\alpha) \ge (c_1\mathbf{C}_a\mathbf{B}_p)^{-1}\left(\eta + \frac{s_a}{|s_a|}c_1\mathbf{C}_a\mathbf{A}_p\mathbf{z}(t-\Delta t)\right), \tag{32}$$

where α is the bound of the variable value, and there is the following relationship:

$$|c_1\mathbf{C}_a\mathbf{A}_p\mathbf{z}(t-\Delta t)| \le \alpha. \tag{33}$$

Since the item $\mathbf{z}(t-\Delta t)$ in Eq. (26) is the state vector that is composed of both modal velocity and modal displacement, it can be obtained from the PZT sensor. However, when only the acceleration sensor is used as the sensor for active vibration suppression, their vectors can not be obtained directly. Thus, Eq. (27) is replaced by an acceleration sensor based combination of nonlinear control algorithm proposed in this paper, and it is expressed as

$$u = -K_{a1} y_a(t-\Delta t) + u_{\mathrm{vss}}, \tag{34}$$

where $K_{a1} > 0$ is the acceleration proportional feedback control gain.

From Eq. (34), we have

$$s_a \dot{s}_a = s_a c_1 y_a(t-\Delta t) = s_a c_1 \mathbf{C}_a(\mathbf{A}_p \mathbf{z}(t-\Delta t) + \mathbf{B}_p u_{\mathrm{vss}} + K_{a1}\mathbf{B}_p y_a(t-\Delta t)) \tag{35}$$

yields

$$y_a(t-\Delta t) = (I - K_{a1}\mathbf{C}_a\mathbf{B}_p)^{-1}\mathbf{C}_a(\mathbf{A}_p\mathbf{z}(t-\Delta t) + \mathbf{B}_p u_{\mathrm{vss}}). \tag{36}$$

Then

$$s_a \dot{s}_a = s_a c_1 (I - K_{a1}\mathbf{C}_a\mathbf{B}_p)^{-1}\mathbf{C}_a(\mathbf{A}_p\mathbf{z}(t-\Delta t) - Q\mathbf{B}_p \operatorname{sgn}(s_a)) \le -\eta|s_a|. \tag{37}$$

To guarantee the stability of the system, the control gain Q should meet the condition of

$$\begin{aligned} Q &\ge (c_1\mathbf{C}_a\mathbf{B}_p)^{-1}(I - K_{a1}\mathbf{C}_a\mathbf{B}_p)(\eta+\beta) \\ &\ge (c_1\mathbf{C}_a\mathbf{B}_p)^{-1}(I - K_{a1}\mathbf{C}_a\mathbf{B}_p)\left(\eta + \frac{s_a}{|s_a|}c_1(I - K_{a1}\mathbf{C}_a\mathbf{B}_p)^{-1}\mathbf{C}_a\mathbf{A}_p\mathbf{z}(t-\Delta t)\right), \end{aligned} \tag{38}$$

where β is the bound of the variable value.

$$|c_1(I - K_{a1}\mathbf{C}_a\mathbf{B}_p)^{-1}\mathbf{C}_a\mathbf{A}_p\mathbf{z}(t-\Delta t)| \le \beta. \tag{39}$$

In the practical implementation of acceleration sensor based control algorithms, signal filters must be introduced because of the large amount of measured noise contained in an acceleration signal. Also, instead of using integration item, a kind of low-pass filter item that has a very small corner frequency is adopted. Then the control bandwidth of the closed-loop system is relatively large. Thus, s_a can be selected as

$$s_a = c_1 y_a(t-\Delta t)\frac{\varepsilon}{s+\varepsilon}\frac{d}{s+d}, \tag{40}$$

where ε is a small positive constant standing for the corner frequency of a first-order low-pass filter; s is Laplace operator; and d is the corner frequency of a first-order low-pass filter to eliminate the high frequency signals measured by acceleration sensor.

And the acceleration sensor based method of combining the proportional feedback and the VSC control is

$$u = -K_{a1} y_a(t-\Delta t)\frac{\omega_f^2}{s^2 + 2\xi_f\omega_f s + \omega_f^2} + u_{\mathrm{vsc}}, \tag{41}$$

where u_{vsc} is the switching variable structure control law. And it can be expressed as

$$u_{\mathrm{vsc}} = -Q\operatorname{sgn}(s_a) = -Q\operatorname{sgn}\left(c_1 y_a(t-\Delta t)\frac{\varepsilon}{s+\varepsilon}\frac{d}{s+d}\right). \tag{42}$$

The proposed control law expressed by Eq. (41) is a kind of acceleration sensor based VSC algorithm.

In addition, there is an exponential trending law. Let the dynamics of the switching function be specified by the differential equation [25]

$$\dot{s}_a = -Q_r \operatorname{sgn}(s_a) - k_r s_a, \tag{43}$$

where Q_r and k_r are the positive constants.

Eq. (43) is the constant plus proportional rate reaching law, and the combination of the switching sliding mode variable structure and the proportional feedback control strategy is designed as

$$u = -Q_r \operatorname{sgn}\left(c_1 y_a(t-\Delta t)\frac{\varepsilon}{s+\varepsilon}\frac{d}{s+d}\right) - k_r c_1 y_a(t-\Delta t)\frac{\varepsilon}{s+\varepsilon}\frac{d}{s+d}. \tag{44}$$

The applied switching control u can be robust to parametric uncertainty and external disturbances.

Remark. For active control of flexible structures, especially, the lower amplitude residual vibration near the equilibrium point is very difficult to be suppressed, which is harmful for stability and attitude control accuracy. In this paper, the VSC algorithm is designed based on non-collocated acceleration sensor measured signal. For the purpose of vibration suppression, the combining controller of the VSC and the proportional feedback control is proposed. The combination of the control scheme makes it possible to suppress both the larger and the lower amplitude vibrations quickly. In this case, the selected control gain of the acceleration proportional control is not so larger, and then the stability and control spillover

of the closed-loop system will not be affected due to much higher control gain. However, for suppressing the lower amplitude vibration, the combined method can supply much larger control effect compared to that of the proportional control. The proposed combined method can not only keep the proportional gain not so high for the larger amplitude vibration, but also keep at a certain control effect for the lower amplitude vibration. Thus, it can suppress the lower amplitude residual vibration quickly. Therefore, the combined method can overcome the problems of the system, such as dead zone nonlinearity. Here, Q is selected to be equal to 20–30 percent of the full control value, meeting the needs for fast suppression of the lower amplitude residual vibration at the equilibrium point.

However, to realize the ideal sliding mode, VSC requires infinite switching frequency which in practice is not achievable due to the limited sampling rate in digital implementation. The finite switching frequency associated with large control gains may cause chattering which may excite the inherent flexible modes [30]. It must be avoided in practical application. To overcome the problem of chattering, a continuous saturation function sat$(*)$ is used to replace the signum function in the controller implementation, which can be formally defined as

$$\mathrm{sat}(*,\sigma)=\begin{cases} */\sigma & \text{if } |*|\le\sigma, \\ */|*| & \text{if } |*|>\sigma. \end{cases} \tag{45}$$

In practical implementation of the proposed control method, the signum function sgn$(*)$ is replaced by sat$(*)$ in Eq. (44). Then the combined control algorithm can be expressed as

$$u=-Q_r\,\mathrm{sat}\left(c_1 y_a(t-\Delta t)\frac{\varepsilon}{s+\varepsilon}\frac{d}{s+d}\right)-k_r c_1 y_a(t-\Delta t)\frac{\varepsilon}{s+\varepsilon}\frac{d}{s+d}. \tag{46}$$

4. Experiments

4.1. Introduction of the experimental test-bed

In order to verify the effectiveness of the proposed non-collocated acceleration sensor based vibration control algorithms, experimental research was conducted on a piezoelectric adaptive graphite/epoxy beam. To implement the proposed non-collocated acceleration feedback control, an experimental setup was erected, as shown in Fig. 6. All sensors and actuators are symmetrically located about the y-axis. The acceleration sensor (type: CA-YD-117, sensitivity: 50 pC/m s^{-2}) is fixed at the beam tip to measure the vibration. The PZT patches are bonded symmetrically on the surface of the beam. The attached PZT patches are close to the clamped side of the beam. In total, there are five PZT patches: one is the PZT sensor and four patches are symmetrically bonded to both sides of the host beam in parallel and are used as a one-channel PZT actuator, as illustrated in Fig. 6.

The control system is implemented by using an industrial personal computer (Pentium IV, CPU 2.4 GHz). The piezoelectric acceleration sensor's signal and the PZT sensor's signal are amplified by charge amplifiers (YE5850) to the voltage range of −10 to +10 V, and converted into digital data through an A/D (analog to digital) card (PCL-818HD,

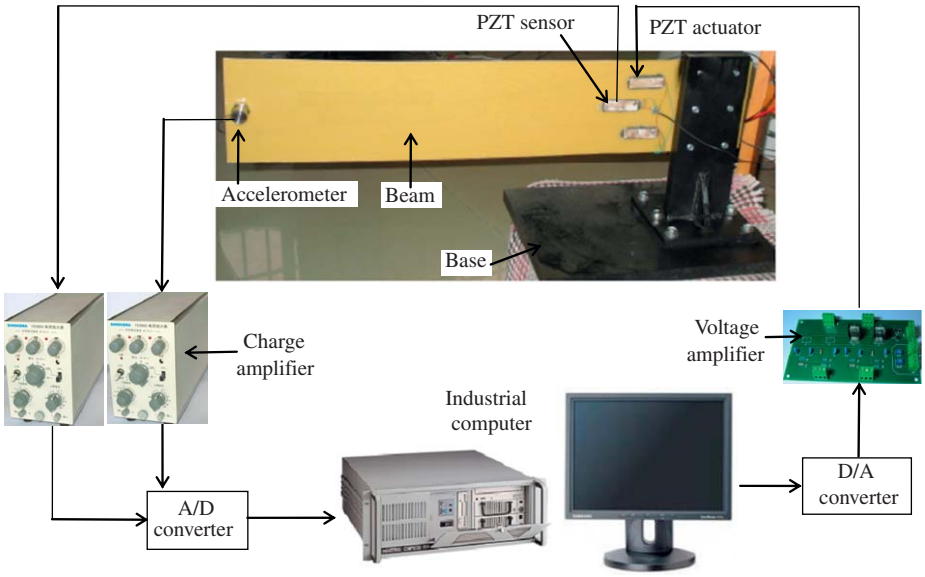

Fig. 6. Photograph of the experimental setup.

16-channel, 12 B). The output of the controller is sent to the amplifier for the PZT actuator, through a D/A (digital to analog) card (PCL-727, 12-channel, 12 B). The piezoelectric actuator is driven by a high voltage amplifier (APEX PA240CX), which amplifies a low voltage signal in the range −5 to +5 V to a high voltage signal in the range −260 to +260 V. The sampling period of the controller is selected as 2 ms.

4.2. Experimental parameters identification

Since the acceleration sensor and the PZT actuator are spatially non-collocated, the phase lag for the second bending mode causes instability problems. Thus, modal phase analysis should be conducted before phase compensation by using phase shifting technology. Phase error identification methods are presented that uses impulse excitation and persistent excitation. In this paper, based on the author's previous work [21,22], phase hysteresis identification for the first and the second bending modes were carried out by impulse excitation and persistent excitation at the resonant frequency. And the hysteresis loops were obtained from the experimental time-domain data that are measured by PZT sensor and the acceleration sensor.

After excitation for the first two bending modes, the time-domain response measured by acceleration sensor is shown in Fig. 7(a). And the frequency response of the first two bending modes can be obtained by employing the fast Fourier transform (FFT), as shown in Fig. 7(b). From Fig. 7(b), it can be seen that the natural frequencies of the first two bending modes are $\omega_1 = 2.50$ Hz and $\omega_2 = 16.41$ Hz, respectively. The determined results are approximately equal to those obtained by FEA in Section 2.2.

In order to analyze the phase hysteresis of the vibration modes between the measured signal of the accelerometer and that of the PZT sensor, the sensitivity of the charge amplifiers for the PZT sensor and the acceleration sensor are adjusted until a good match between their measured amplitude is obtained. To filter out the high frequency noise, the signals measured by both the PZT sensor and the accelerometer are filtered by the same low-pass filter. The reason for using the same filter is that the phase lags caused by the low-pass filter are equal for both signals. Then, the practical phase error due to non-collocated placement can be accurately obtained. Since the control design model consists of only the first two modes, the corner frequency of the filter is selected as 35 Hz.

The phase hysteresis of the non-collocated acceleration sensor and PZT actuator is identified by excitation analysis. Because the PZT sensor and the PZT actuator are nearly collocated, their phase error is relatively small, and so it can be ignored. Thus, the phase error of the measured signals between the accelerometer and the PZT sensor is approximately equal to that of the accelerometer and the PZT actuator. Therefore, the phase lag parameters can be obtained by experimental identification.

To obtain the phase lag angle between the signal measured by the PZT sensor and that by acceleration sensor, excitation analysis is conducted. After impulse excitation for the first bending mode, the time-domain response of the first bending mode measured by the PZT sensor and the acceleration sensor are shown in Fig. 8(a) and (b), respectively. And the magnitude frequency responses of the first bending mode are obtained by employing FFT, as shown in Fig. 9(a) and (b), respectively. By using these two measured signals as the *X*- and the *Y*-coordinate, one can plot the Lissajou figure with decayed damping behavior response, as shown in Fig. 10(a). From Fig. 10(a), one can know that the non-collocated placement will cause a decayed phase hysteresis loop for the first bending mode. And the decayed curve-fitting Lissajou figure can be smoothened by the following equations:

$$\begin{cases} x = 8.0\exp(-2\pi\xi_1\omega_1 t)\sin(2\pi\omega_1 t), \\ y = 8.0\exp(-2\pi\xi_1\omega_1 t)\sin(2\pi\omega_1 t + \phi_1), \end{cases} \tag{47}$$

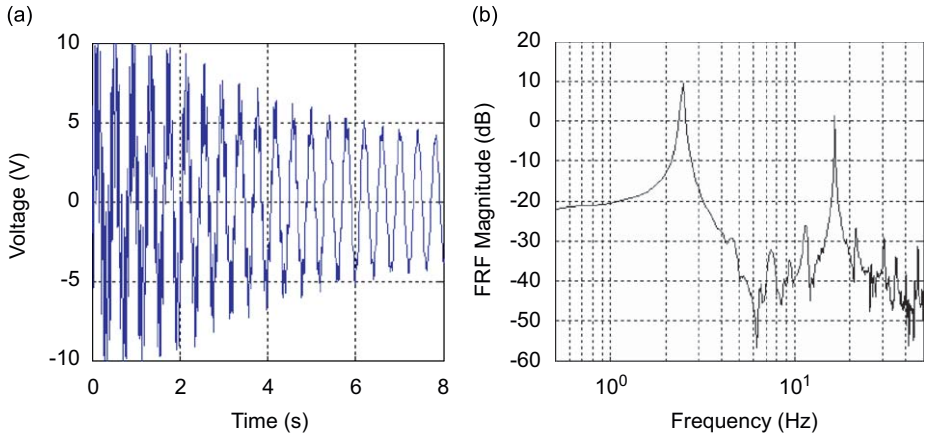

Fig. 7. The first two bending modes' vibration measured by the accelerometer: (a) time-domain response and (b) frequency-domain response.

where the natural frequency is $\omega_1 = 2.50\,\text{Hz}$; the damping ratio is $\xi_1 = 0.0052$; and the phase error is $\phi_1 = -0.93\,\text{rad}$, that is to say, $\phi_1 = -53.28^\circ$.

By employing Eq. (47) as the *X*- and the *Y*-coordinate, another decayed curve-fitting Lissajou figure can be obtained as shown in Fig. 10(b). Comparing Fig. 10(a) with (b), it can be seen that they are well matched. Thus, the phase lag angle of the first bending mode can be obtained from Eq. (47), and it is $\phi_1 = -53.28^\circ$.

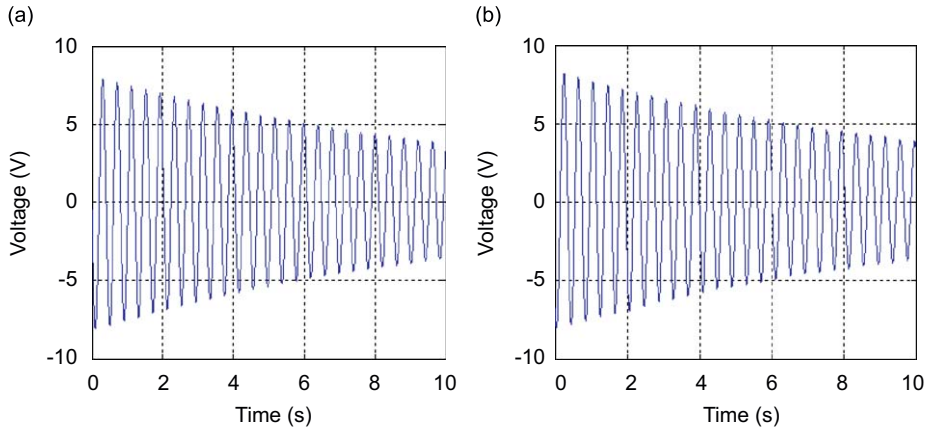

Fig. 8. Time-domain response of the first bending mode: (a) PZT patch sensor measured signal and (b) acceleration sensor measured signal.

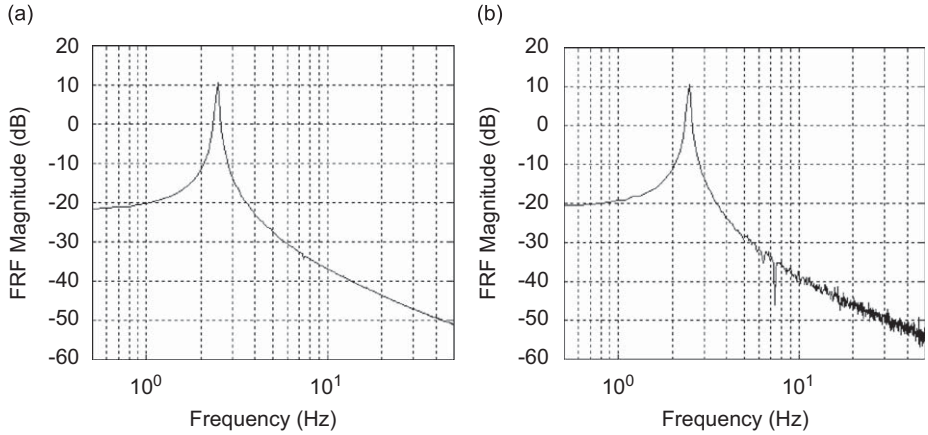

Fig. 9. Frequency response of the first bending mode: (a) PZT patch sensor measured signal and (b) acceleration sensor measured signal.

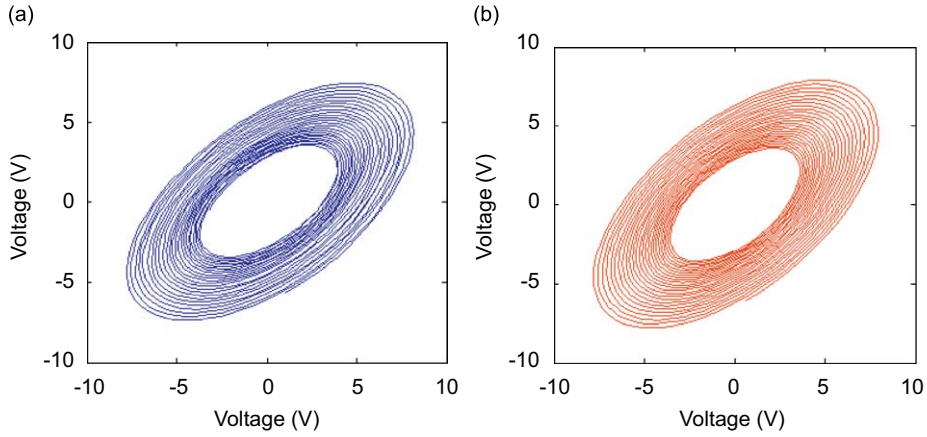

Fig. 10. Lissajou figures between the signals of acceleration sensor and PZT sensor: (a) measured signals and (b) curve fitting.

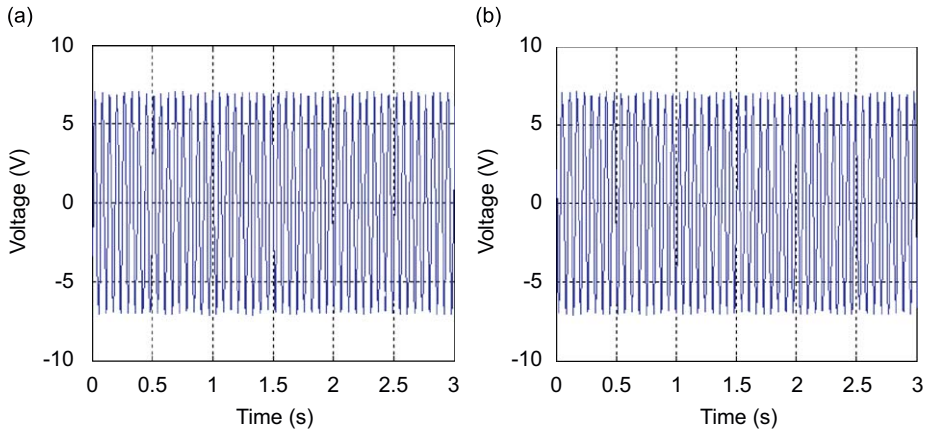

Fig. 11. Persistent exciting response of the second bending mode: (a) PZT patch sensor measurement and (b) acceleration sensor measurement.

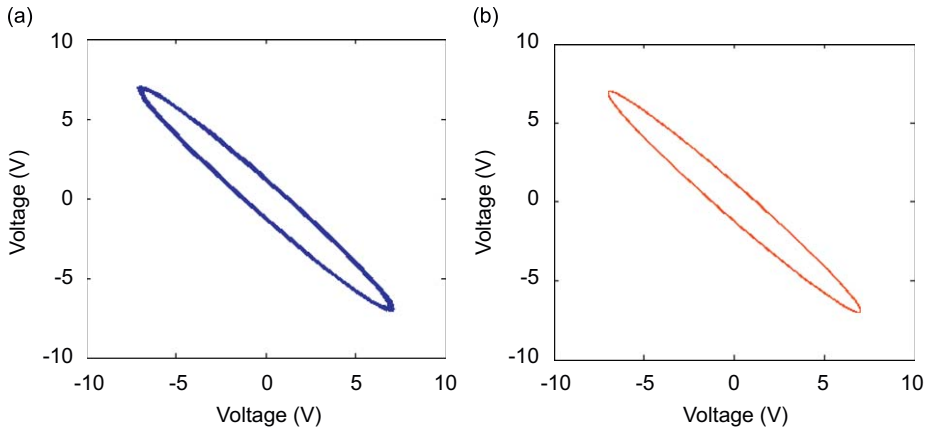

Fig. 12. Lissajou figures between the signals measured by acceleration sensor and PZT sensor: (a) Lissajou experimental figure and (b) Lissajou curve fitting figure.

To obtain the phase error of the second bending mode, persistent excitation analysis is conducted. The PZT actuator is used to excite persistent vibration of the flexible beam by voltage amplifier. The excited signal is generated by the signal generator at the second bending mode's resonant frequency, i.e., $\omega_2 = 16.41$ Hz. When the excited vibration of the second bending mode is stable and its amplitude remains at a certain value, one can record the experimental data measured by the acceleration sensor and the PZT sensor for a period of three seconds. The vibration signals measured by the PZT and the accelerometer sensor are shown in Fig. 11(a) and (b), respectively. By using these two signals as the *X*- and the *Y*-coordinate, one can plot the Lissajou figure, as shown in Fig. 12(a). From Fig. 12(a) one can know that the non-collocated placement will cause a phase hysteresis for the second bending mode, and the hysteresis loop resembles an ellipse. The curve-fitting Lissajou figure for the second bending mode is smoothened by the following equations:

$$\begin{cases} x = 7.0\ \sin(2\pi\omega_2 t), \\ y = 7.0 \sin(2\pi\omega_2 t + \phi_2), \end{cases} \tag{48}$$

where the natural frequency is $\omega_2 = 16.41$ Hz; and the phase error is $\phi_2 = -2.97$ rad, that is to say, $\phi_2 = -170.2^\circ$.

By employing Eq. (48) as the *X*- and the *Y*-coordinate, another curve-fitting Lissajou figure can be obtained as shown in Fig. 12(b). Comparing Fig. 12(a) with (b), it can be seen that they are approximately the same. Thus, the phase lag angle of the second bending mode can be obtained from Eq. (48), and the phase lag angle is equal to -170.2°.

According to the above-identified results, the phase lag of the non-collocated placement of the acceleration sensor and the PZT actuator for the first bending mode is $\phi_1 = -53.28^\circ$. Thus, the time delay of the first bending mode is

$$\Delta t_1 = \frac{\phi_1}{360^\circ} \times \frac{1000}{\omega_1} = -59.2\ \text{ms}. \tag{49}$$

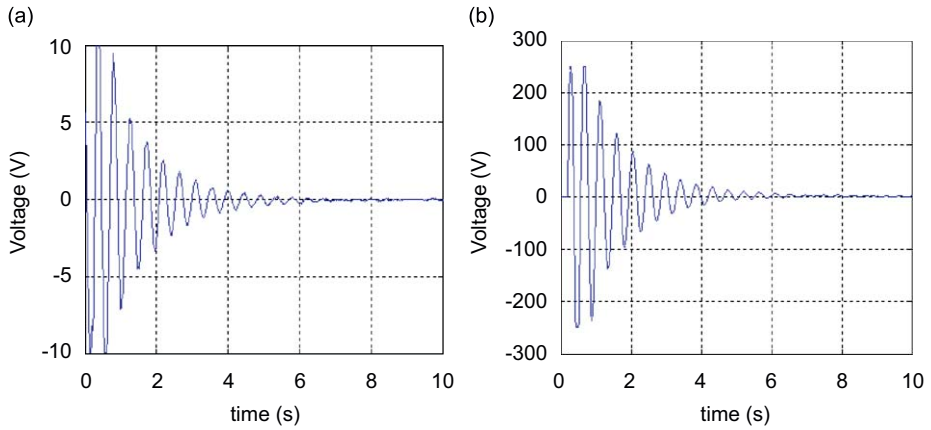

Fig. 13. Response of the first bending mode with acceleration proportional feedback control: (a) time-domain response and (b) control voltage.

For the second mode, the phase lag between the signals measured by the accelerometer and the PZT sensor is $\phi_2 = -170.2^\circ$, and the phase lag time for the second mode is

$$\Delta t_2 = \frac{\phi_2}{360^\circ} \times \frac{1000}{\omega_2} = -28.8\,\text{ms}. \tag{50}$$

The energy of the flexible beam system is concentrated in the first two bending modes. For active control of the first two bending modes, the phase error due to the non-collocated placement of the sensor and the actuator should be compensated for. By utilizing phase shifting technology to tune the phase lag of the second mode to zero, the phase lag time of the first mode is still $-59.2-(-28.8) = -30.4$ ms. Therefore, the phase lag is still

$$\Delta\phi_1 = \frac{-30.4\,\text{ms}}{-59.2\,\text{ms}} \times (-53.28^\circ) = -27.36^\circ \tag{51}$$

for the first bending mode. Thus, the control stability and performance will not be affected.

According to the above analysis, when the tuning time is selected as $\Delta t = 28.8$ ms in the controller design, the phase lag due to the non-collocated placement of the acceleration sensor and the PZT actuator can be compensated, for the first two bending modes.

4.3. Experimental vibration control research

In order to verify the effectiveness of the proposed acceleration sensor based control method, experimental comparison research was conducted, including acceleration proportional feedback control and the combined VSC control for the first bending mode and then for the first two bending modes.

The time-domain closed-loop vibration responses of the first and the first two bending modes dampened by the acceleration proportional output feedback control algorithm of Eq. (15) are shown in Figs. 13(a) and 14(a), respectively. And their control voltages applied to the PZT actuators for the first and the first two bending modes are shown in Figs. 13(b) and 14(b), respectively. From the experimental results, it can be seen that the acceleration proportional feedback control algorithm can suppress the larger vibration amplitude significantly, but the lower vibration amplitude near equilibrium point will last for a long period of time to disappear.

The time-domain vibration responses of the first and the first two bending modes controlled by Eq. (44) are shown in Fig. 15(a) and (b), respectively. From the results, one can know that the combined VSC methods with the switching surface will cause control chattering at the equilibrium point. To solve this problem, saturation function is used to replace the switching function.

The time-domain closed-loop vibration responses of the first and the first two bending modes dampened by Eq. (46) are shown in Figs. 16(a) and 17(a), respectively. And their control voltages applied to the PZT actuators for the first and the first two bending modes are shown in Figs. 16(b) and 17(b), respectively. From the experimental results, one can know that the control chattering is disappeared.

In the control voltage plots as shown in Figs. 16(b) and 17(b), the saturation signals can be found. The saturation points are at the peak value of the vibration signal. Only the full control value is applied. Because the peak value vibrations need full control effect, this will not cause chattering due to the limited energy of the actuator at peak value vibration. However, it is different from the VSC method by Eq. (44) used in this paper. The VSC caused control chattering as shown in Fig. 15 is due to the high frequency on–off control effect at the equilibrium point; and its control value is less than the full control value.

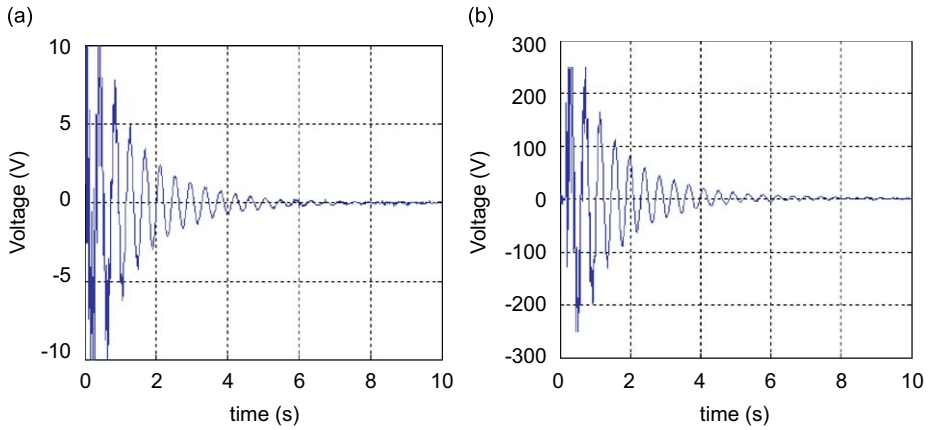

Fig. 14. Response of the first two bending modes with acceleration proportional feedback control: (a) time-domain response and (b) control voltage.

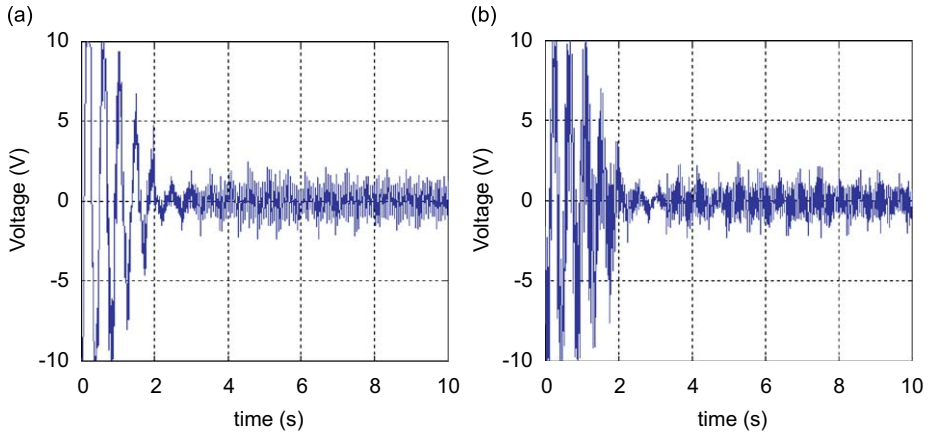

Fig. 15. Response of the acceleration based switching VSC control: (a) the first bending mode and (b) the first two bending modes.

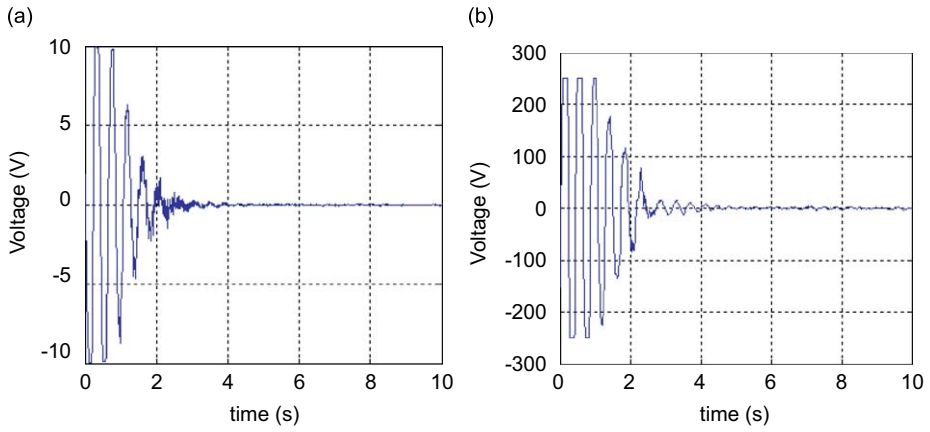

Fig. 16. Response of the first bending mode with acceleration based saturation VSC control: (a) time-domain response and (b) control voltage.

From the experimental results, it is known that the non-collocated acceleration sensor feedback control can suppress the vibration effectively. However, the experimental results have shown that the simple acceleration sensor based proportional feedback control strategies do not guarantee satisfactory performances. The experimental results by using the acceleration sensor based VSC methods are better than those by using acceleration proportional feedback control. Time

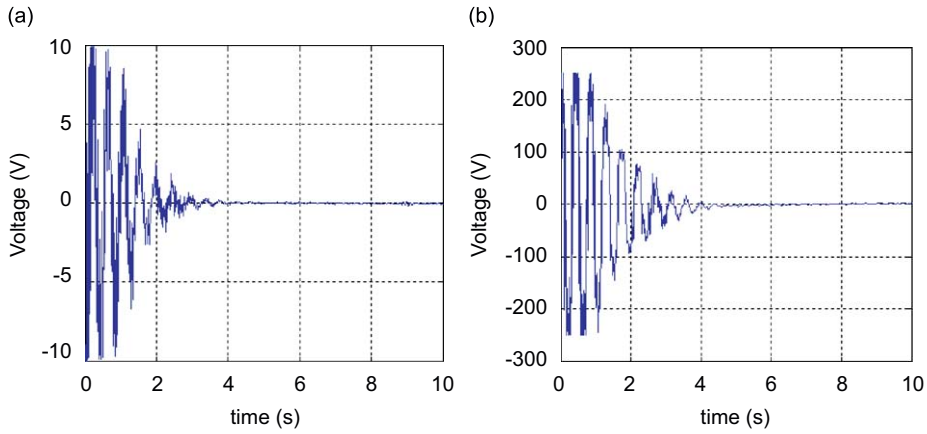

Fig. 17. Response of the first two bending modes with acceleration based saturation VSC control: (a) time-domain response and (b) control voltage.

required for the vibration to decay and disappear by means of acceleration proportional feedback is longer than that of the VSC method. It is a significant finding that the proposed acceleration sensor based VSC control method can suppress both the larger and the lower amplitude bending vibrations quickly, especially, for the lower amplitude vibration suppression quickly. The improvements of the proposed acceleration sensor based VSC control algorithm have been verified experimentally. However, if the time delay is neglected in control design, this will cause instability and the divergent oscillation of the high frequency modal vibration especially of the second bending mode.

5. Conclusion

This paper presents the theoretical analysis and experimental results of active vibration suppression of a flexible beam with bonded discrete PZT patch sensor/actuators and mounted accelerometer. Acceleration sensor based proportional feedback control and sliding mode variable structure control algorithms are used to actively control the vibration of a beam, and their stability is theoretically analyzed and experimentally verified. A second-order low-pass filter is introduced to eliminate the phenomenon of control spillover and to filter out the noises of the measured acceleration signal. To compensate for the phase hysteresis due to the non-collocated placement of the PZT actuator and the acceleration sensor, phase shifting technology is applied to the controller that employs experimentally determined parameters. Experimental research is conducted to compare the results of the different control methods. And it is shown that the first two bending modes of the beam are effectively suppressed by the proposed methods. The experimental results confirm the effectiveness and robustness of the presented acceleration sensor based control strategies.

Acknowledgments

This research work was partially supported by the National Natural Science Foundation of China under Grants 60404020 and 90505014; and this project was partially supported by State Key Laboratory of Robotics Foundation (no. RLO200805). The first author gratefully acknowledges these support agencies. The authors would like to thank the anonymous reviewers for their constructive comments and suggestions which made substantial improvements to this paper.

References

[1] K. Worden, W.A. Bullough, J. Haywood, *Smart Technologies*, World Scientific, Singapore, 2003.
[2] D.C. Hyland, J.L. Junkins, R.W. Longman, Active control technology for large space structures, *Journal of Guidance, Control and Dynamics* 16 (5) (1993) 801–821.
[3] D. Sun, J.K. Mills, J.J Shan, S.K. Tso, A PZT actuator control of a single-link flexible manipulator based on linear velocity feedback and actuator placement, *Mechatronics* 14 (4) (2004) 381–401.
[4] T. Bailey, J.E. Hubbard, Piezoelectric-polymer active vibration control of a cantilever beam, *Journal of Guidance, Control and Dynamics* 8 (5) (1985) 605–611.
[5] C.R. Fuller, S.J. Elloitt, P.A. Nelson, *Active Control of Vibration*, Academic Press, San Diego, CA 92101, 1996.
[6] P. Gardonio, S.J. Elliott, Modal response of a beam with a sensor–actuator pair for the implementation of velocity feedback control, *Journal of Sound and Vibration* 284 (1-2) (2005) 1–22.
[7] X.J. Dong, G. Meng, J.C. Peng, Vibration control of piezoelectric smart structures based on system identification technique: numerical simulation and experimental study, *Journal of Sound and Vibration* 297 (3–5) (2006) 680–693.
[8] S.X. Xu, T.S. Koko, Finite element analysis and design of actively controlled piezoelectric smart structures, *Finite Elements in Analysis and Design* 40 (3) (2004) 241–262.
[9] C.J. Goh, T.K. Caughey, On the stability problem caused by finite actuator dynamics in the collocated control of large space structures, *International Journal of Control* 41 (3) (1985) 787–802.

[10] J.L. Fanson, T.K. Caughey, Positive position feedback control for large space structures, *AIAA Journal* 28 (4) (1990) 717–724.
[11] A. Baz, S. Poh, Experimental implementation of the modified independent modal space control method, *Journal of Sound and Vibration* 139 (1) (1990) 133–149.
[12] S.N. Singh, R. Zhang, Adaptive output feedback control of spacecraft with flexible appendages by modeling error compensation, *ACTA Astronautic* 54 (4) (2004) 229–243.
[13] P. Shimon, E. Richer, Y. Hurmuzlu, Theoretical and experimental study of efficient control of vibrations in clamped square plate, *Journal of Sound and Vibration* 282 (1–2) (2005) 453–473.
[14] J.H. Yang, F.L. Lian, L.C. Fu, Nonliear adaptive control for flexible-link manipulators, *IEEE Transactions on Robotics and Automation* 13 (1) (1997) 140–148.
[15] J. Lin, An active–passive absorber by using hierarchical fuzzy methodology for vibration control, *Journal of Sound and Vibration* 304 (3–5) (2007) 752–768.
[16] Z.C. Qiu, X.M. Zhang, H.X. Wu, et al., Optimal placement and active vibration control for piezoelectric smart flexible cantilever plate, *Journal of Sound and Vibration* 301 (3–5) (2007) 521–543.
[17] T. Singh, W. Singhose, Input shaping/time delay control of maneuvering flexible structures, *Proceedings of the American Control Conference*, Archorage, AK, May 8–10, 2002, pp. 1717–1731.
[18] J. Shan, D. Sun, D. Liu, Design for robust component synthesis vibration suppression of flexible structures with on–off actuators, *IEEE Transactions on Robotics and Automation* 20 (3) (2004) 512–525.
[19] R.H. Cannon, E. Schmitz, Initial experiments on the end-point control of a flexible one-link robot, *International Journal of Robotics Research* 3 (3) (1984) 62–75.
[20] D. Sun, J. Shan, Y.X. Su, et al., Hybrid control of a rotational flexible beam using enhanced PD feedback with a nonlinear differentiator and PZT actuators, *Smart Materials & Structures* 14 (1) (2005) 69–78.
[21] L. Meirovitch, *Dynamics and Control of Structures*, Wiley, New York, 1990, p. 327.
[22] S.S. Ge, T.H. Lee, G. Zhu, F. Hong, Variable structure control of a distributed-parameter flexible beam, *Journal of Robotic Systems* 18 (1) (2001) 17–27.
[23] M.C. Pai, A. Sinha, Sliding mode output feedback control of vibration in a flexible structure, *Transactions of the ASME, Journal of Dynamic Systems, Measurement and Control* 129 (6) (2007) 851–855.
[24] J.J. Slotine, W.P. Li, *Applied Nonlinear Control*, Prentice-Hall, Englewood Cliffs, New Jersey, 1991.
[25] J.Y. Hung, W.B. Gao, J.C. Hung, Variable structure control: a survey, *IEEE Transactions on Industrial Electronics* 40 (1) (1993) 2–22.
[26] S.B. Choi, J.W. Sohn, Chattering alleviation in vibration control of smart beam structures using piezofilm actuators: experimental verification, *Journal of Sound and Vibration* 294 (3) (2006) 640–649.
[27] B. Bandyopadhyay, T.C. Manjunath, M. Umapathy, *Modeling Control and Implementation of Smart Structures*, Springer, Berlin, Heidelberg, 2007.
[28] A. Preumont, *Vibration Control of Active Structures*, Kluwer Academic Publishers, Dordrecht, 2004.
[29] Q.L. Hu, G.F. Ma, L.H. Xie, Robust and adaptive variable structure output feedback control of uncertain systems with input nonlinearity, *Automatica* 44 (2) (2008) 552–559.
[30] W.J. Cao, J.X. Xu, A learning variable structure controller of a flexible one-link manipulator, *Journal of Dynamic Systems, Measurement, and Control* 122 (4) (2000) 624–631.
[31] Q.L. Hu, G.F. Ma, Spacecraft vibration suppression using variable structure output feedback control and smart materials, *Journal of Vibration and Acoustics, Transactions of the ASME* 128 (2) (2006) 221–230.
[32] P.T. Kotnic, S. Yurkovich, et al., Acceleration feedback for control of a flexible manipulator arm, *Journal of Robotic Systems* 5 (3) (1988) 181–195.
[33] G. Gatti, M.J. Brennan, P. Gardonio, Active damping of a beam using a physically collocated accelerometer and piezoelectric patch actuator, *Journal of Sound and Vibration* 303 (3–5) (2007) 798–813.
[34] J.D. Han, Y.Q. He, W.L. Xu, Angular acceleration estimation and feedback control: an experimental investigation, *Mechatronics* 17 (9) (2007) 524–532.
[35] W.L. Xu, J.D. Han, Joint acceleration feedback control for robots: analysis, sensing and experiments, *Robotics and Computer-Integrated Manufacturing* 16 (5) (2000) 307–320.
[36] E. Dumetz, J.Y. Dieulot, P.J. Barre, T. Delplace, Control of an industrial robot using acceleration feedback, *Journal of Intelligent Robot System* 46 (2) (2006) 111–128.
[37] S.V. Gosavi, A.G. Kelar, Modeling, identification, and passivity-based robust control of piezo-actuated flexible beam, *Journal of Vibration and Acoustics, Transactions of the ASME* 126 (2) (2004) 260–271.
[38] S. Chatterjee, Vibration control by recursive time-delayed acceleration feedback, *Journal of Sound and Vibration* 317 (1–2) (2008) 67–90.
[39] Z.C. Qiu, Active vibration control for flexible smart structure based on acceleration feedback, *Chinese Journal of Mechanical Engineering* 44 (3) (2008) 143–151 (in Chinese).
[40] Z.C. Qiu, Acceleration sensor based active control for piezoelectric adaptive beam structure, *Proceedings of the Seventh International Symposium on Test and Measurement*, Beijing, China, pp. 2784–2787.
[41] G.P. Cai, S.X. Yang, A discrete optimal control method for a flexible cantilever beam with time delay, *Journal of Vibration and Control* 12 (5) (2006) 509–526.
[42] K.K. Tan, S.Y. Lim, T.H. Lee, H. Dou, High-precision control of linear actuators incorporating acceleration sensing, *Robotics and Computer Integrated Manufacturing* 16 (5) (2000) 295–305.
[43] C.C. Cheng, P.W. Wang, Applications of the impedance method on multiple piezoelectric actuators driven structures, *Journal of Vibration and Acoustics, Transactions of the ASME* 123 (2) (2001) 262–268.
[44] Y. Sakawa, F. Matsuno, S. Fukushima, Modeling and feedback control of a flexible arm, *Journal of Robotic Systems* 2 (4) (1985) 453–472.
[45] A. Bonchis, P.I. Corke, D.C. Rye, Q.P. Ha, Variable structure methods in hydraulic servo systems control, *Automatica* 37 (4) (2001) 589–595.